TORNADO IN SOUTH-WESTERN LUXEMBOURG ON 9 AUGUST 2019:

METEOROLOGICAL CONTEXT AND DAMAGE ASSESSMENT

Date	02/07/2020
Author	Luca Mathias
Version	1.0
Number of pages	30

TABLE OF CONTENTS

1. INTRODUCTION.....3
2. DATA AND METHODS.....5
3. SYNOPTIC-SCALE OVERVIEW.....7
4. MESOSCALE STORM ENVIRONMENT.....8
5. STORM CELL ANALYSIS.....12
6. TORNADO TRACK AND DAMAGE ASSESSMENT.....18
7. SUMMARY AND CONCLUSIONS.....24
ACKNOWLEDGEMENTS.....25
REFERENCES.....25

1. INTRODUCTION

On 9 August 2019, an intense thunderstorm crossed over the south-western part of the Grand Duchy of Luxembourg during the evening hours and produced a significant tornado along its path. Severe tornadic wind damage was reported in Rodange, Lamadelaine, Pétange and Bascharage (cf. Fig. 1). For instance, roughly 400 trees and a total of 310 houses were damaged in Bascharage, 50 of which lost their roofs (Gemeng Käerjeng 2019). 80 people had to be sheltered in hotels or other accommodations. Moreover, the tornado was associated with 17 minor casualties and 2 seriously injured persons. In the aftermath of this extreme weather event, the total insured losses were estimated to be at least 100 million Euros.

Recent studies have shown that tornadoes can be observed everywhere in Europe (Groenemeijer and Kühne 2014, Antonescu et al. 2016, Antonescu et al. 2017). On average, 200 to 300 tornadoes occur over pan-European land each year. In addition, these studies revealed that roughly 70 % of European tornadoes are weak (F0 or F1), about 29 % are strong (F2 or F3) and only 1 % of the reported tornadoes reach a violent intensity (F4 or F5). Examples of strong tornadoes near Luxembourg in the past are the tornado in the Belgian town Léglise on 20 September 1982 (Caniaux 1984) and the tornado in the German city of Trier on 7 October 1988 (Trierischer Volksfreund 2008). Between 1950 and 2013, tornadoes caused 316 fatalities in Europe (Antonescu et al. 2017). The European tornado season spans primarily from late spring (Eastern Europe) over midsummer (Central and Western Europe) to late summer and early autumn (Mediterranean region).

The aforementioned high impacts in south-western Luxembourg motivate a detailed investigation of this hazardous weather event. Hence, the purpose of this case study is to analyse the synoptic and mesoscale environment in which the tornado-producing thunderstorm was initiated and developed, and to describe its characteristics by means of radar and lightning data.

This article is structured as follows: Section 2 describes the data used in this study and an overview of the large-scale atmospheric conditions will be provided in section 3. The mesoscale environment will be examined in section 4, which comprises a thorough discussion of the factors favouring tornadogenesis. An analysis of the tornadic storm cell is given in section 5. Section 6 includes an assessment of the tornado damage. A short summary and conclusions are provided in the last section.

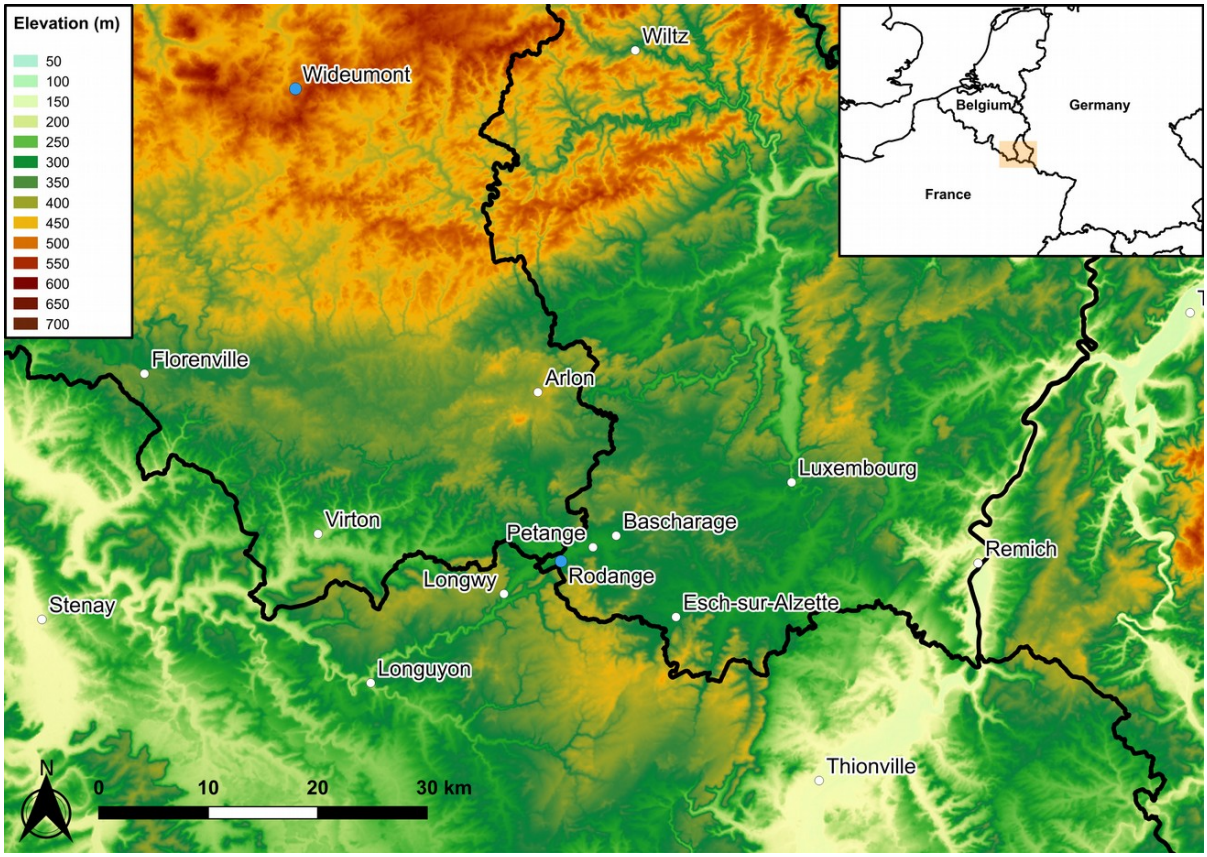

Figure 1: Topographic map of the investigation area (shaded orange in the inset on the upper-right-hand side). The blue dots denote the meteorological radar located in Wideumont and the automated weather station located in Rodange.

2. DATA AND METHODS

To analyse the near-surface environment in the vicinity of the tornado, in situ measurements from an automated surface weather station located in Rodange "um Clopp" operated by the Kachelmann Group (KG) are considered. The station data has a temporal resolution of 10 minutes. Moreover, data from the operational C-band radar in Wideumont operated by the Royal Meteorological Institute of Belgium (RMIB) is used to document the mesoscale evolution of the storm. The Doppler radar performs a multiple elevation scan every 5 minutes with a beam width of one degree and a horizontal resolution of 250 m in range. Reflectivity-only elevation scans have a maximum range of 250 km, whereas combined reflectivity-velocity elevation scans have a smaller maximum coverage of 125 km. The antenna of the radar is installed at a height of 590 m above mean sea level (AMSL). The radar data is processed and visualized using the freely available software NLradar[1].

In addition to the in situ and remote sensing data, numerical weather prediction (NWP) model data will be analysed. Operational analysis data from the European Centre for Medium-Range Weather Forecasts (ECMWF) will be used to examine the synoptic-scale atmospheric conditions. The analysis was produced using 4D-Var data assimilation with the model cycle 46r1 of ECMWF's Integrated Forecast System (IFS). The operational analysis data output has a native horizontal grid spacing of approximately 9 km and 137 levels in the vertical. The mesoscale tropospheric environment will be examined using the convection-resolving limited-area NWP model Applications de la Recherche à l'Opérationnel à Mésoéchelle (AROME; Seity et al. 2011) operated by Météo-France and operationally used by MeteoLux. AROME has a native horizontal grid interval of 1.3 km and 90 vertical levels. The initial and lateral boundary conditions for AROME are provided by the global NWP model Action de Recherche Petite Echelle Grande Echelle (ARPEGE; Courtier et al. 1991) which is also operated by Météo-France. AROME's simulation initialised at 12:00 UTC on 9 August 2019 is considered as the reference simulation in this study because of the realistic representation of the evolution of the prefrontal mesoscale surface low (see sections 3 and 4 for more details). The following severe convective weather parameters were calculated using hourly surface and pressure level data from AROME:

- Storm-Relative Helicity (SRH) after Bunkers et al. (2000):

$$SRH = \int_{z_1}^{z_2} \left[(\vec{v} - \vec{c}) \cdot \vec{\omega} \right] dz$$

1 https://www.weerwoord.be/m/2429671

where z_1 is the bottom level, z_2 is the top level, $\vec{v}$ is the wind vector, $\vec{c}$ is the storm motion vector and $\vec{\omega}$ is the horizontal vorticity vector.

For a right-moving storm the storm motion vector is calculated as follows:

$$\vec{c} = \vec{v}_{mean} + 7.5 \left[\frac{\vec{v}_{shear} \times \hat{k}}{\left| \vec{v}_{shear} \right|} \right]$$

where $\vec{v}_{mean}$ is the 0-6 km mean wind vector, $\vec{v}_{shear}$ is the 0-6 km vertical wind shear vector and $\hat{k}$ is the vertical unit vector.

- Updraft Helicity (UH) after Kain et al. (2008):

$$UH = \int_{z_1}^{z_2} (w\zeta)\, dz$$

where z_1 is the bottom level, z_2 is the top level, w is the non-hydrostatic vertical velocity and ζ is the vertical vorticity.

- Supercell Composite Parameter (SCP) after Thompson et al. (2004):

$$SCP = \frac{MUCAPE}{1000\ J\,kg^{-1}} \cdot \frac{SRH_{0-3km}}{50\ m^2 s^{-2}} \cdot \frac{DLS}{20 m\, s^{-1}}$$

where the deep layer shear (DLS) is the 0-6 km bulk shear and the most unstable convective available potential energy (MUCAPE) is computed for the most unstable parcel located between the surface and the level where the pressure equals 0.7 times the surface pressure (Groenemeijer et al. 2019).

- WMAXSHEAR after Taszarek et al. (2017):

$$WMAXSHEAR = DLS\sqrt{2 \cdot MUCAPE}$$

Lastly, lightning data from the European Cooperation for Lightning Detection (EUCLID) network will be considered as well. The location accuracy of the EUCLID network ranges from 100 to 700 m and the detection efficiency for cloud-to-ground (CG) lightning flashes is greater than 93 % (Schulz et al. 2016). Intra-cloud (IC) discharges are also captured by the EUCLID network, but with a much lower and highly variable detection efficiency in the range of 10 to 50 % (Pédeboy et al. 2014, Schulz et al. 2014).

3. SYNOPTIC-SCALE OVERVIEW

At 12:00 UTC on 9 August 2019, an upper-air ridge extended from Algeria over the Alps to Denmark and an upper-level low was located near Ireland (Fig. 2a). This synoptic-scale pattern resulted in a strong south-westerly flow in the mid to upper troposphere over Western Europe (Fig 2a). A cyclonically curved jet streak with maximum wind speeds of 65 to 70 m s^{-1} was situated over the French region Brittany to the north-west of the Bay of Biscay (Fig. 2a). The mid- to upper-tropospheric low corresponded to a deep surface low centred near the south-west coast of Ireland (Fig. 2b). The cold front associated with this low extended from the North Sea to the Iberian Peninsula and the air mass within the warm sector was characterised by a high moisture content, especially in the vicinity of the prefrontal surface pressure trough over northern France with total column water vapour values of up to 50 mm (Fig. 2b). This air mass originated from the subtropical North Atlantic basin, since the cyclogenesis occurred slightly to the north of the Azores. As the orientation of the cold front relative to the upper-level flow had a strong parallel component, it moved relatively slow eastward and crossed Luxembourg between 18:00 and 19:00 UTC.

When comparing this large-scale pattern to the one observed during the tornado outbreak in Western Europe in June 1967 (Dessens and Snow 1989, Antonescu et al. 2020), similarities were found among the location of the vertically stacked low pressure system and among the presence of a prefrontal pressure trough superposed by a strong south-westerly flow in the middle troposphere. Contrarily to this case, the synoptic regime during the severe tornadic storm in northern France on 3 August 2008 was strongly forced (Tuschy 2009, Wesolek and Mahieu 2011).

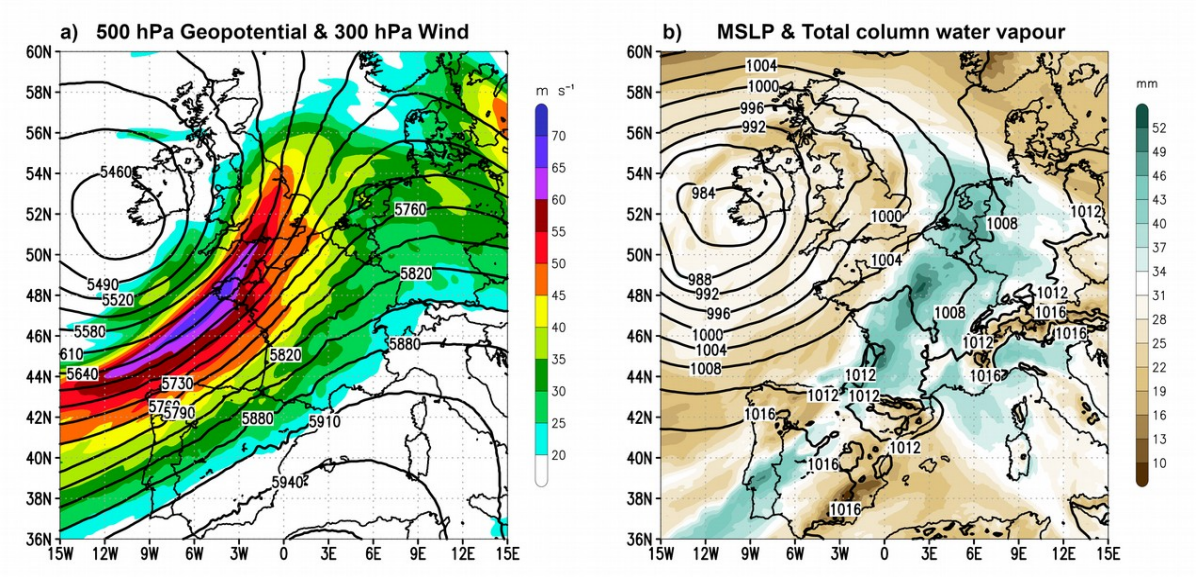

Figure 2: ECMWF analysis of the synoptic-scale conditions on 9 August 2019 at 12:00 UTC over Western Europe. (a) 500 hPa geopotential height (black lines; gpm) and 300 hPa wind speed (shaded; m s^{-1}). (b) Mean sea level pressure (black lines; hPa) and total column water vapour or precipitable water (shaded; mm).

4. MESOSCALE STORM ENVIRONMENT

The low-level conditions were characterised by a prefrontal mesoscale low pressure area over northern France between 12:00 and 15:00 UTC on 9 August 2019 (Fig. 3a). This area was covered by a subtropical air mass with 925 hPa wet-bulb potential temperatures ranging from 20 to 23 °C (Fig. 3a) and low-level water vapour mixing ratios of 12 to 15 g kg^{-1} (Fig. 4). The combination of the enhanced boundary layer moisture and a conditionally unstable lapse rate between the surface and 600 hPa (Fig. 5) resulted in a regionally varying MUCAPE between 500 and 1500 J kg^{-1} (Fig. 3b). An area-averaged vertical profile at 13:00 UTC of the region, where the tornadic thunderstorm intensified (cf. dashed black outlined box in Fig. 3; see section 5 for further details), revealed a relatively thin CAPE distribution over a large part of the very moist tropospheric column, with very low CAPE within the lowest 3 km (Fig. 4). Lastly, a sufficiently strong lifting mechanism to overcome the initially significant convective inhibition (CIN; see Fig. 4) was likely provided by low-level convergence zones in the surrounding area of the mesoscale surface low, which completes the list of necessary ingredients for the development of deep moist convection (Johns and Doswell 1992).

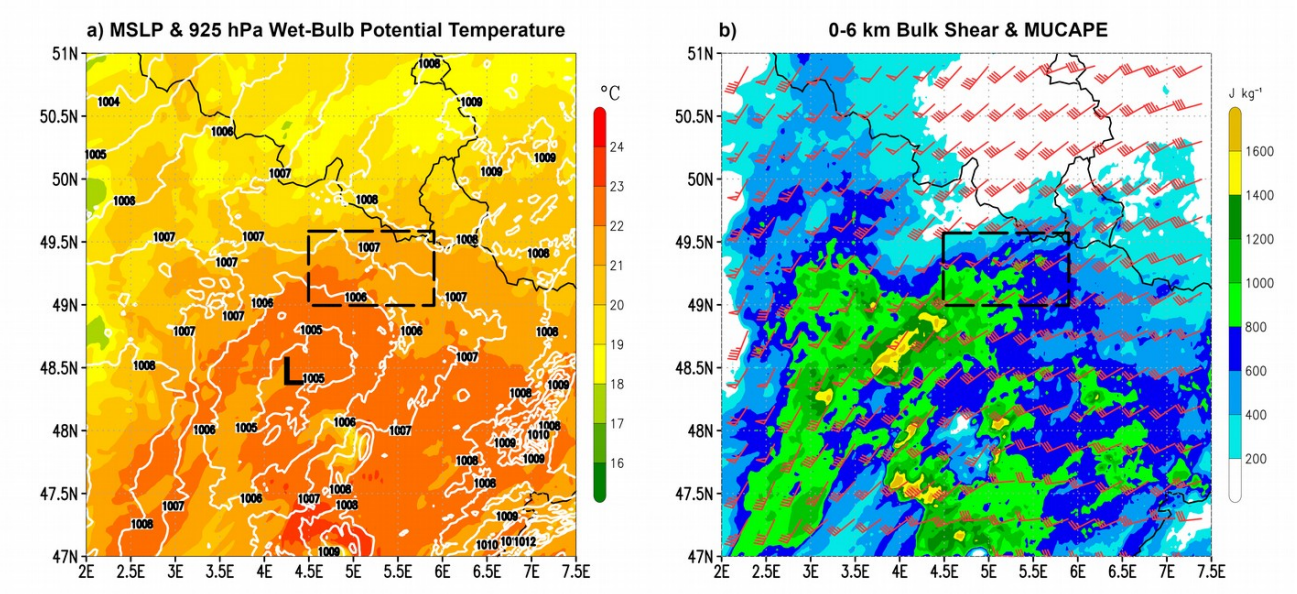

Figure 3: Forecast of the pre-convective environment for 13:00 UTC on 9 August 2019 by the 12:00 UTC run of AROME. (a) Mean sea level pressure (white lines; hPa) and 925 hPa wet-bulb potential temperature (shaded; °C). (b) 0-6 km bulk shear (red wind barbs; knots) and most-unstable CAPE (shaded; J kg^{-1}). The mesoscale low is denoted by the black "L" in (a). The dashed black outlined box in (a) and (b) indicates the area considered for the vertical profile shown in Fig. 4.

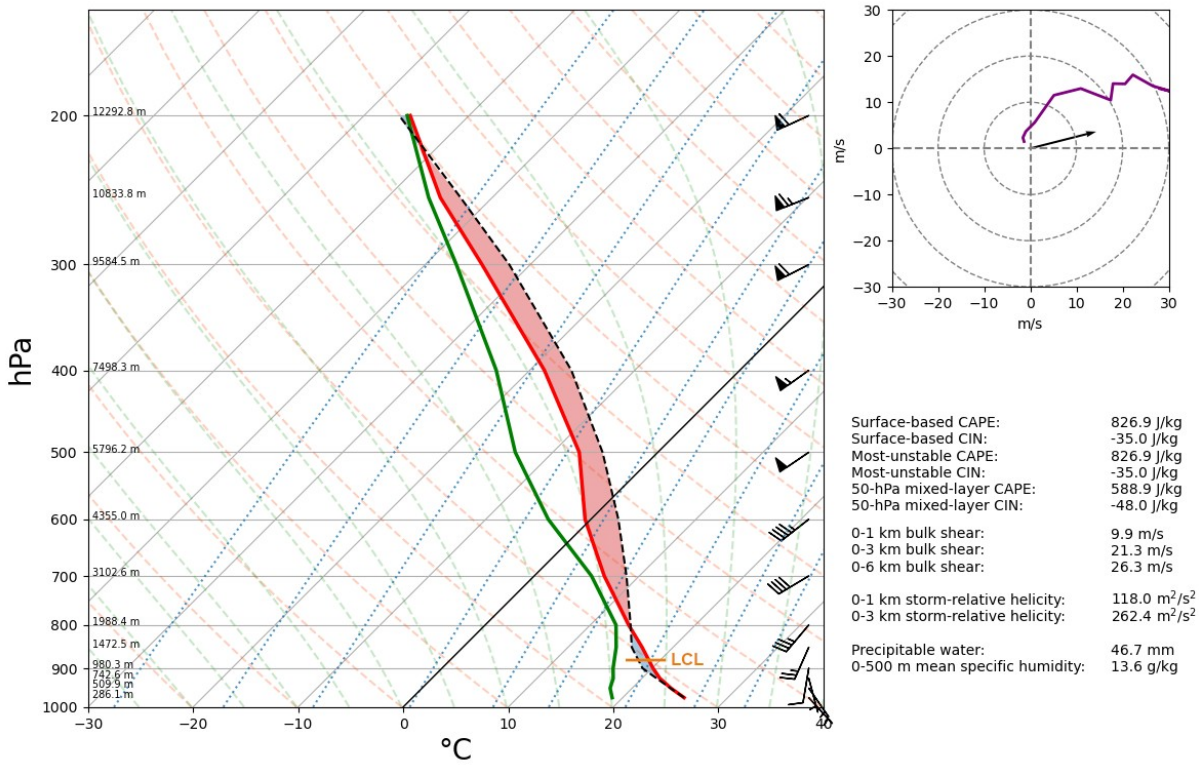

Figure 4: Skew-T log-p diagram of an area-averaged vertical profile (area is denoted by the dashed black box in Fig. 3) at 13:00 UTC on 9 August 2019. The red (green) curve represents the temperature (dew point) and the dashed black curve represents the ascent trajectory of the most unstable parcel. The most-unstable CAPE (CIN) is indicated by the area shaded in transparent red (blue). The black arrow in the hodograph represents the storm motion of a right-moving supercell computed after Bunkers et al. (2000). The lifted condensation level (LCL) marks the expected cloud base of a convective storm. The wind barbs are displayed in knots (1 kt = 0.5144 m s^{-1}).

To determine the dominant storm mode, the vertical shear of wind speed and direction is analysed, since it is a crucial ingredient for well organised deep moist convection producing severe weather (e.g., Rasmussen and Blanchard 1998, Púčik et al. 2015, Taszarek et al. 2017). Firstly, very strong 0-6 km bulk shear with values exceeding 20 m s^{-1} overlapped with the prevailing latent instability over north-eastern France and Luxembourg (Fig. 3b), resulting in WMAXSHEAR values ranging mostly from 600 to 1200 m^2 s^{-2} with regional maxima exceeding 1400 m^2 s^{-2} (not shown). However, most of the 0-6 km bulk shear was concentrated in the layer below 3 km or 700 hPa, whereas the 0-1 km bulk shear values were around 10 m s^{-1} (Fig. 4).

In addition to the strong speed shear, significant veering of the wind was apparent below 700 hPa (Fig. 4), especially along the northern flank of the mesoscale surface low where easterly winds prevailed. Thus, large 0-3 km SRH values of 200 to 300 m^2 s^{-2} were present over eastern Belgium, Luxembourg and parts of north-eastern France between 12:00 and 15:00 UTC, with more isolated pockets of up to 400 m^2 s^{-2} (Fig. 5a). Overall, the prevailing regime of weak to moderate latent instability, high shear and helicity generally allows the development of supercell thunderstorms with a deep and persistently rotating updraft (mesocyclone). Hence, enhanced values of the SCP were evident over parts of northern France close to Luxembourg (not shown). The reference simulation of AROME indeed showed multiple, rather discrete storm cells with updraft helicity values exceeding 100 m^2 s^{-2} over northern France at 14:00 UTC (Fig. 5b), thus hinting at the increased likelihood for the occurrence of isolated supercells.

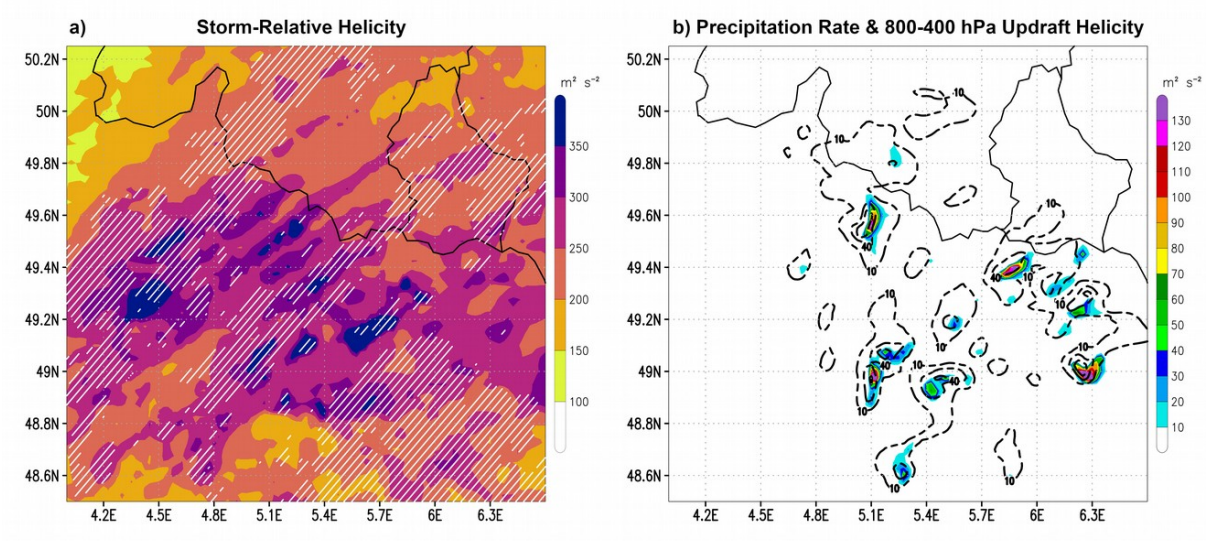

Figure 5: Forecast by the 12:00 UTC run of AROME. (a) Maximum 0-3 km storm-relative helicity (shaded; m^2 s^{-2}) and 0-1 km storm-relative helicity above 100 m^2 s^{-2} (white hatched areas) between 12:00 and 15:00 UTC on 9 August 2019. (b) Precipitation rate (dashed black lines; mm h^{-1}) and updraft helicity between 800 and 400 hPa (shaded; m^2 s^{-2}) for 14:00 UTC on 9 August 2019.

The tornadic potential of the supercell storms was significant due to enhanced values of 0-1 km SRH (100 to 150 m^2 s^{-2}) over parts of northern France, eastern Belgium and Luxembourg (Fig. 5a). However, it is important to underline the potentially large variability of low-level helicity on a temporal and/or spatial scale (Markowski et al. 1998), meaning that the area-averaged 0-1 km SRH value at 13:00 UTC shown in Fig. 4 is possibly not representative for the environment near the tornadic storm. Moreover, the high relative humidity within the boundary layer corresponded to a low cloud base height of 1000 to 1500 m AMSL (cf. Fig 4) and to a less negatively buoyant cold pool of the storm due to decreased evaporational cooling. These moist and strongly sheared conditions at lower levels tend to favour tornadogenesis under a sufficiently strong mesocyclone as shown by numerous studies (e.g. Thompson et al. 2003, Markowski and Richardson 2009, Markowski and Richardson 2014a, Markowski and Richardson 2014b, Coffer and Parker 2017, Yokota et al. 2018).

The aforementioned mesoscale tropospheric conditions compare reasonably well with the environment during the Western European tornado outbreak in June 1967 (Dessens and Snow 1989, Antonescu et al. 2020). However, in contrast to the violent tornado event in northern France in August 2008 (Tuschy 2009, Wesolek and Mahieu 2011), the SRH and bulk shear values were significantly lower in this case.

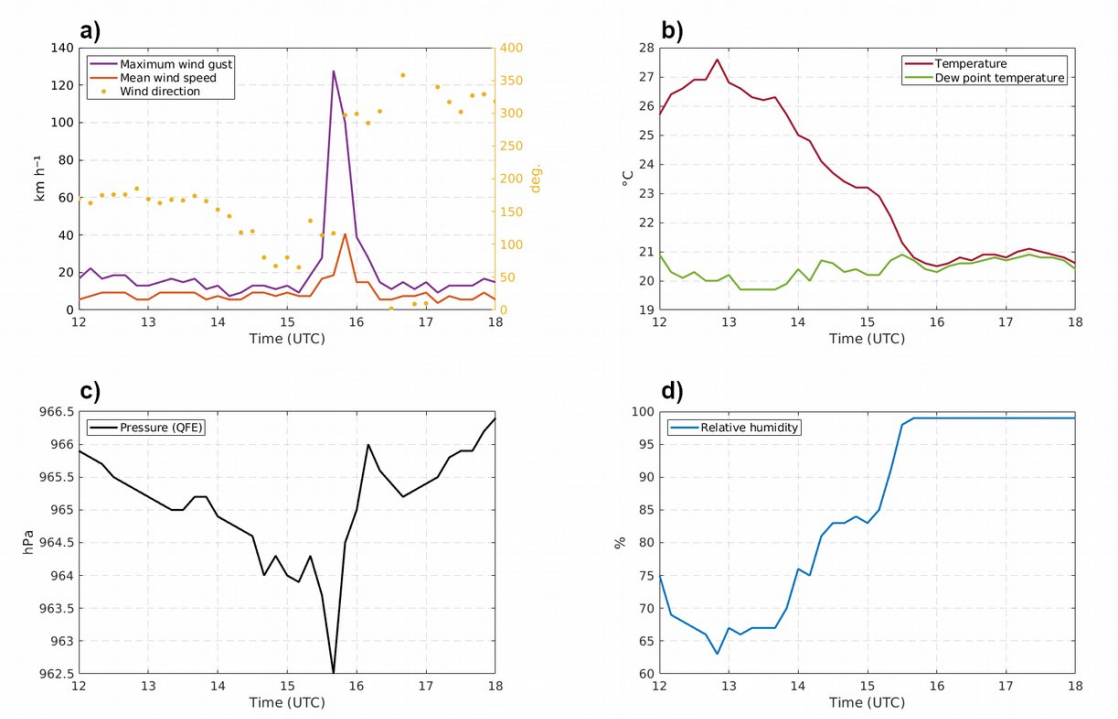

Figure 6: In situ measurements from the automated weather station located in Rodange (cf. Fig. 1) between 12:00 and 18:00 UTC on 9 August 2019. (a) Maximum wind gusts (purple line; km h^{-1}) and mean wind speed (orange line; km h^{-1}) during the preceding 10 minutes (1 km h^{-1} = 0.278 m s^{-1}), and corresponding mean wind direction (yellow dots; °). (b) Instantaneous temperature (red line, °C) and dew point temperature (green line, °C) measured 2 m above the ground. (c) Instantaneous surface pressure (black line; hPa). (d) Instantaneous relative humidity (blue line; %) measured 2 m above the ground.

A sample of parameters measured at the surface within the tornadic environment was provided by an automated weather station located in Rodange in south-western Luxembourg, which was hit by the circulation of the tornado between 15:30 and 15:45 UTC (Fig. 6). Prior to the passage of the tornadic storm (14:30 to 15:30 UTC), the temperature steadily decreased with the onset of precipitation while the dew point temperature remained between 20 and 21 °C, resulting in an increase of the relative humidity to values of 80 to 90 % (cf. Figs. 6b with 6d). The pressure also decreased slightly due to the approach of the mesoscale low and the wind blew from easterly directions (varying between 65° and 120°) with a mean speed of 2 to 3 m s^{-1} (Figs. 6a,c). When the tornadic storm hit the station, the temperature decreased by approximately 2 °C and the dew point temperature did not change, hinting at a weak cold pool (Fig. 6b). Furthermore, the wind veered rapidly to north-westerly directions and a peak gust of 35.5 m s^{-1} was measured at 15:40 UTC (Fig. 6a). The relatively sharp pressure drop observed at 15:40 UTC was caused by the pressure perturbation of the tornadic wind circulation (Fig. 6b).

5. STORM CELL ANALYSIS

At 12:00 UTC on 9 August 2019, a major supercellular thunderstorm developed to the south-east of Paris in northern France and moved east-north-eastwards (path of feature “S1” in Fig. 7a), while producing a substantial amount of lightning flashes and reaching the northern part of the German state Saarland by 16:00 UTC. This supercell showed a remarkable structure in the radar reflectivity data with a 60-dBZ echo top height of approximately 9 km and a maximum reflectivity of 68 dBZ in roughly 7 km altitude at 14:00 UTC (not shown). It produced hail and severe non-tornadic wind gusts along its path (28.2 m s^{-1} measured in the French towns Châlons-Vatry and Rouvres-en-Woëvre).

Between 12:00 and 14:00 UTC, a large-scale precipitation field with embedded and mostly weak convective cells formed in the adjacent north-west sector of the isolated supercell storm (cf. lightning activity north of “S1” in Fig. 7a). When this major storm reached the French city Verdun around 14:40 UTC, a second supercellular storm started to form slightly to the north-west (path of feature “S2” in Fig. 7a). At 15:00 UTC, a relatively broad rotational circulation within that storm became apparent in the radial velocity data at an altitude of about 2 to 3 km with maximum inbound velocities of 35 to 40 m s^{-1} and maximum outbound velocities of 2 to 5 m s^{-1} (black circle in Fig. 8). Subsequently, the 50-dBZ echo top reached a height of approximately 7 km by 15:05 UTC due to the rapid strengthening of the mesocyclonic updraft, coinciding with a significant increase of the intra-cloud lightning (Figs. 7a,b).

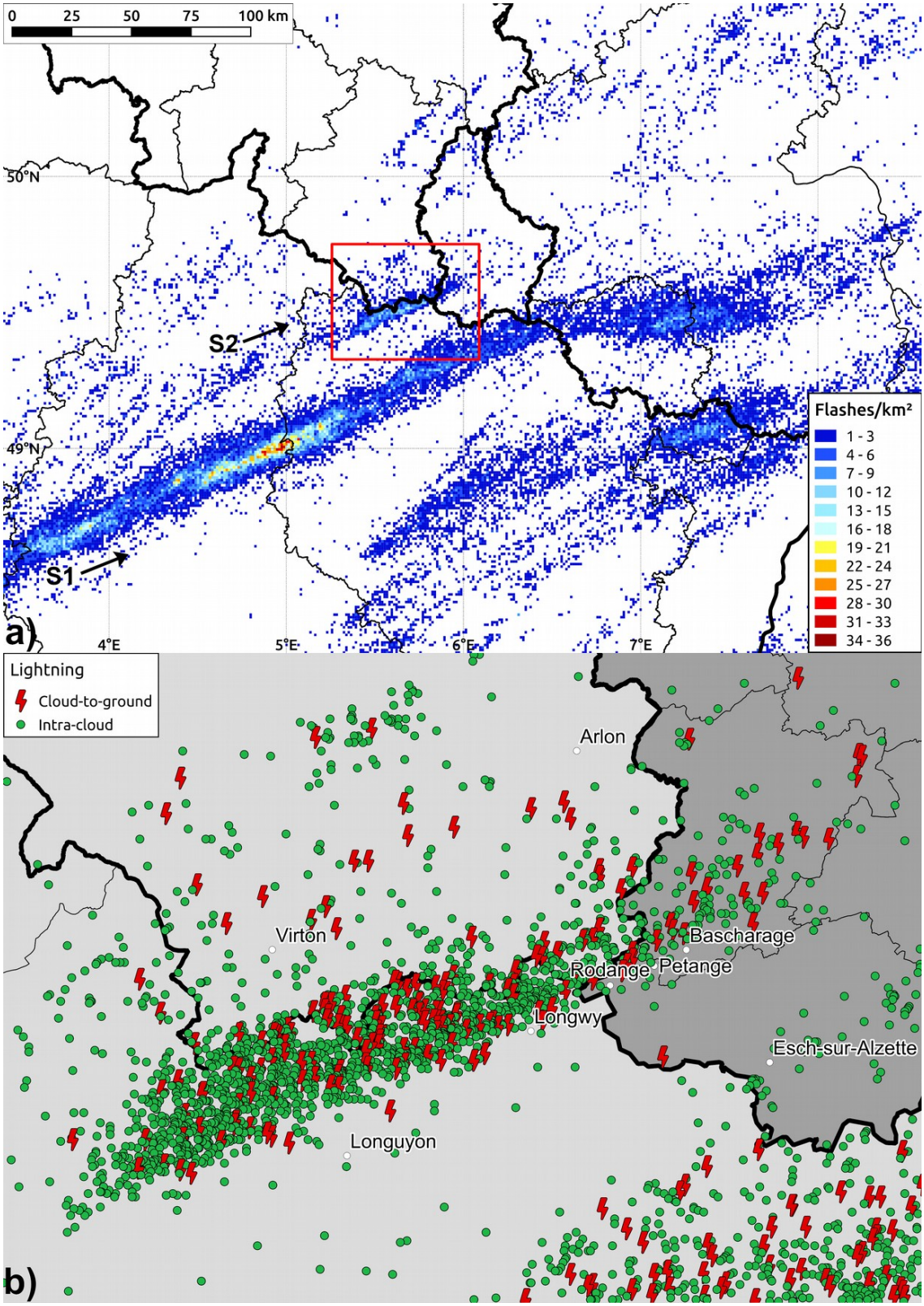

Figure 7: (a) Spatial distribution of the lightning density (flashes per km^2) on 9 August 2019. The red box denotes the area shown in (b). The features "S1" and "S2" are mentioned in the text. (b) Spatial distribution of cloud-to-ground and intra-cloud lightning flashes between 15:00 and 16:00 UTC.

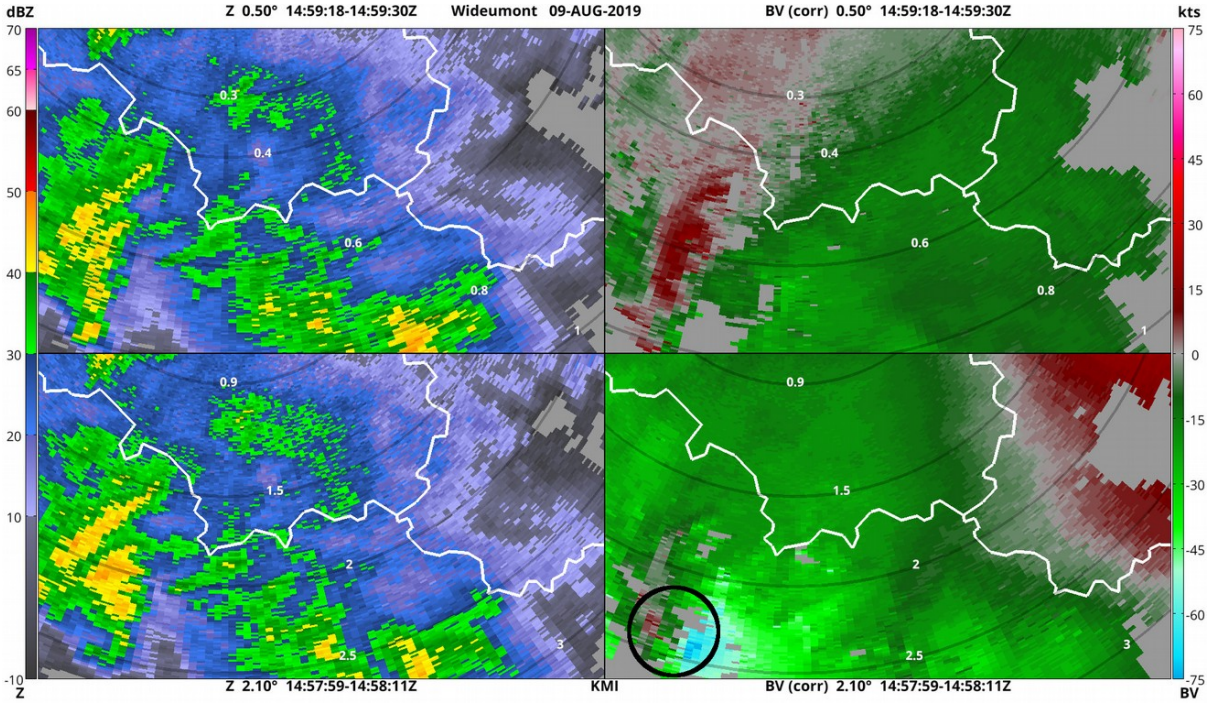

Figure 8: Base reflectivity (dBZ) and corrected base radial velocity (kts; 1 kt = 0.5144 m s^{-1}) of the 0.5° elevation scan (upper panel) and the 2.1° elevation scan (lower panel) performed by the RMIB radar located in Wideumont at about 15:00 UTC on 9 August 2019. The grey concentric circles indicate the height (km) of the radar beam. The black circle in the lower right panel denotes the mesocyclone. Negative velocities indicate a relative movement towards the radar and positive velocities indicate a relative movement away from the radar.

As the supercell reached the Franco-Belgian border at 15:15 UTC, the reflectivity scans revealed a V-shaped form of the precipitation field associated with the forward-flank downdraft (FFD) of the storm (Fig. 9a). A well-defined mesocyclone was again found at lower levels in the velocity scans (black circle in Fig. 9a), corresponding to a bounded weak echo region (BWER) from about 2.5 to 5 km altitude in the reflectivity data. However, the lowest elevation scan did not show a clear rotational circulation yet (cf. upper right panel in Fig. 9a). While the storm moved along the Franco-Belgian border producing a lot of lightning flashes (Fig. 7), a distinct hook echo showed up at the southern tip of the supercell in the low-level reflectivity scan at around 15:25 UTC (Fig. 9b). Furthermore, the radial velocity scan at the lowest elevation angle revealed a signature of rotation at an altitude of about 1 km, although significant filtering is obvious in the centre of the circulation (dark blue circle in Fig. 9b). This may suggest that the lower part of the mesocyclone strengthened between 15:15 and 15:25 UTC, tornadogenesis occurring during the 10 subsequent minutes. The narrow 50-dBZ core of the storm, which was superposed to the low- to mid-level mesocyclone, extended to a height of 8 km, whereas the 18-dBZ echo top height reached up to about 12 km at 15:25 UTC (not shown).

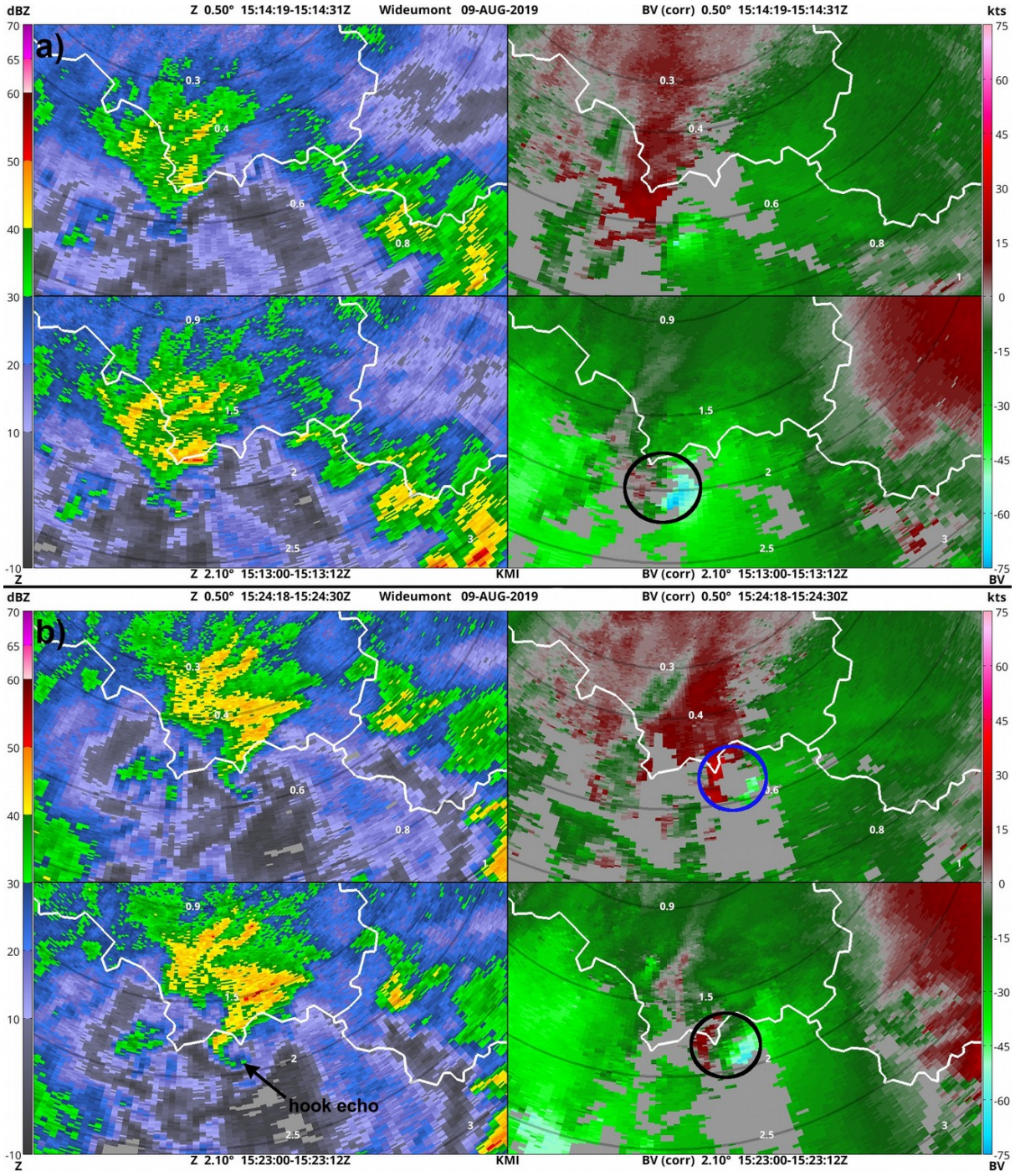

Figure 9: Same as in Fig. 8 but for about (a) 15:15 UTC and (b) 15:25 UTC on 9 August 2019. The black circle in the lower right panels of (a) and (b), and the dark blue circle in the upper right panel of (b) denote the mesocyclone.

The hook echo of the supercell storm reached the French town Longwy at about 15:35 UTC (Fig. 10a), where the storm likely entered its major tornadic phase. The mesocyclone was still evident in the radial velocity data. The scan at the lowest elevation angle revealed an azimuthal shear couplet with inbound velocities of about 23 m s^{-1} and outbound velocities of about 17 m s^{-1} (dark blue circle in Fig. 10a), representing the base of the mesocyclone associated with the tornado at the surface. Since filtering was again very prominent in the centre of the vortex signature (Fig. 10a), the probably strongest part of the mesocyclonic circulation could not be analysed. Between 15:40 and 15:45 UTC, the vortex reached the Luxembourgish town Bascharage. A clear velocity couplet was again visible in the imagery at an altitude of roughly 1 km (dark blue circle in Fig. 10b). At that moment, however, the supercell storm started to weaken as the lightning density decreased significantly (cf. Fig. 7), suggesting that the mesocyclonic updraft was collapsing. Shortly thereafter the tornado rapidly dissipated. The potential causes for the dissipation were the weakening of the low-level mesocyclone by 15:50 UTC and the occlusion of the rear-flank downdraft (RFD), which was indicated by the narrowing of the weak-echo slot associated with the hook echo (cf. Figs. 10a with 10b). The remnants of the supercell then passed slightly north of the capital Luxembourg City between 15:55 and 16:10 UTC, producing only sporadic lightning flashes (cf. Fig. 7). Overall, the supercell storm travelled a distance of approximately 100 km while producing the tornado at the end of its life cycle.

Regarding the performance of the mesocyclone detection algorithm (MCD; Wapler et al. 2016, Hengstebeck et al. 2018) developed by the German Weather Service (DWD), the mesocyclone of the supercell was well detected over the period from 15:05 to 15:15 UTC (not shown). The algorithm assigned the severity level 3 to the mesocyclone, which indicates a deep and moderately strong mesocyclonic rotation. At 15:15 UTC the mesocyclone had a depth of approximately 6 km, a diameter of roughly 10 km and a maximum rotational velocity of about 17 m s^{-1} according to the analysis output of the MCD. In the following, the algorithm struggled to detect the precise location of the mesocyclone. The detections at 15:25 UTC, 15:35 UTC and 15:40 UTC were all displaced to the north by about 5 to 10 km relative to the actual location of the vortex (not shown). In general, mesocyclones detected by the MCD may sometimes not be adequately sampled by a single radar alone (cf. Hengstebeck et al. 2018), which could limit the use of the MCD for Luxembourg and the surrounding regions in some cases, as only the radar located Neuheilenbach contributes to the mesocyclone detection over that territory.

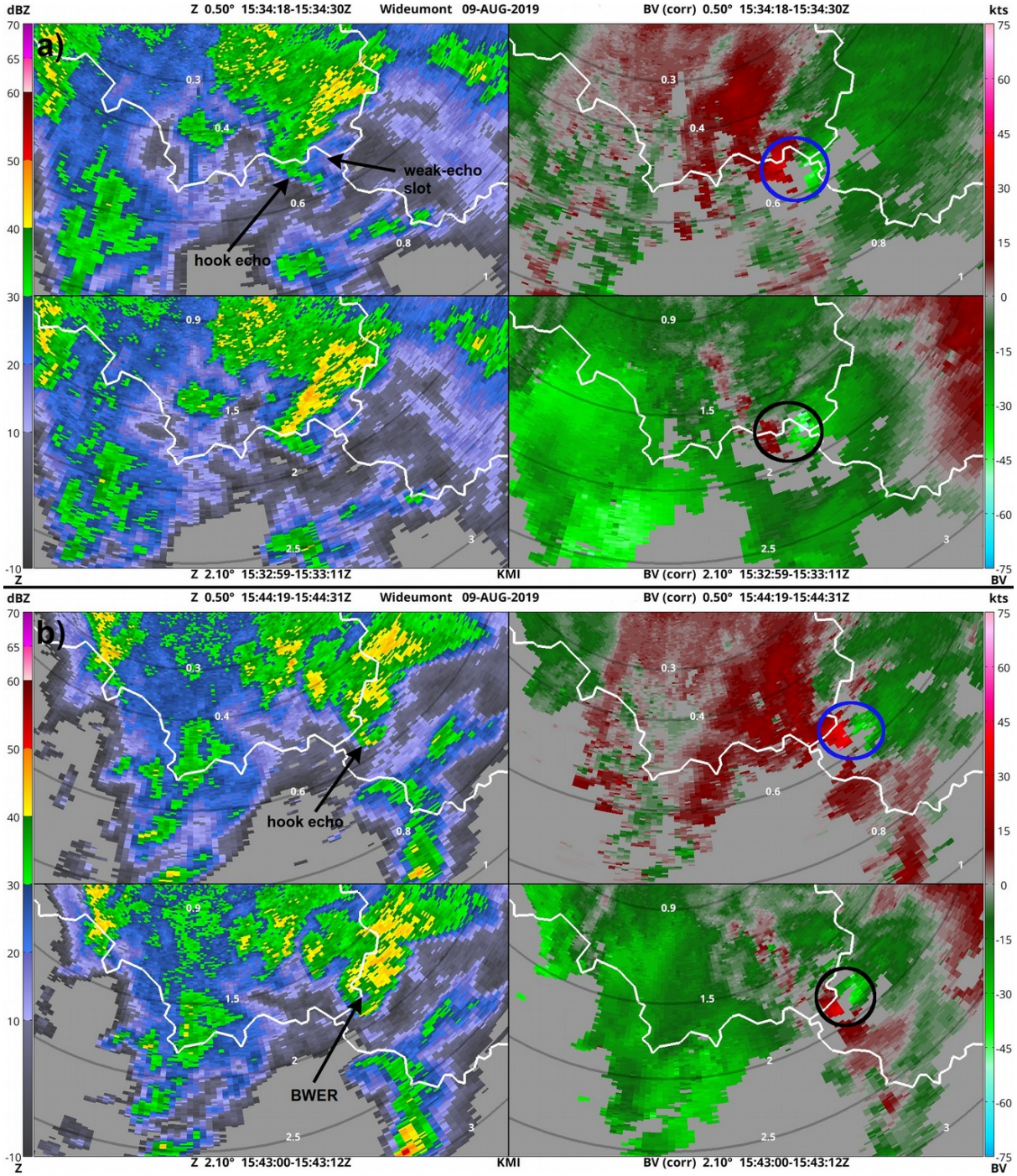

Figure 10: Same as in Fig. 8 but for about (a) 15:35 UTC and (b) 15:45 UTC on 9 August 2019. The black an dark blues circles in the lower and upper right panels of (a) and (b) denote the mesocyclone.

6. TORNADO TRACK AND DAMAGE ASSESSMENT

The analysis of the tornado track shown in Fig. 11 is based on media reports, witness reports, storm chaser reports and on a detailed damage documentation for the town of Bascharage mapped by the technical department of the municipality of Käerjeng. The damage rating of the tornado is based on the International Fujita (IF) scale currently in development by a steering group lead by the European Severe Storms Laboratory (Groenemeijer et al. 2018).

The first damage associated with the tornado was detected slightly to the west of Longwy by a French storm chaser team[2]. Some damage was even detected further to the south-west of Longwy in the town of Montigny-sur-Chiers[3], but this could not be clearly linked to the tornado. When passing through the towns of Longwy and Herserange around 15:35 UTC, the tornado already reached IF1 intensity (cf. Fig. 11 and Fig. 12). As the tornado moved north-eastward, it remains unclear if the vortex weakened temporarily between Herserange and Rodange. However, after the tornado crossed the border from France to Luxembourg, it quickly gained strength and reached IF2 intensity in Lamadelaine, where numerous houses lost their roofs. The vortex maintained this strong intensity while passing through densely populated areas of Pétange and Bascharage (cf. Fig. 11 with Figs. 13 to 18). The tornado even produced debris projectiles, which hit the walls of some houses and remained stuck to them. Furthermore, the damage path of the tornadic circulation widened from approximately 350 m to 750 m (excluding extreme damage location outliers) while passing through Bascharage from the south-west to the north-east, indicating that the tornado adopted a multi-vortex structure, which was confirmed by multiple eyewitness videos. While exiting Bascharage towards the north-east, the tornado weakened abruptly. Finally, the last minor damage to vegetation was visible in Schouweiler, suggesting that the tornado completely dissipated between Schouweiler and Dippach around 15:45 UTC (Fig. 11). A lot of debris lifted up by the tornado in Pétange and Bascharage was found in Schouweiler and Dippach.

Overall, the mesocyclonic tornado lasted for about 10 to 15 minutes and travelled a distance of approximately 18 to 20 km. The estimated translation speed of the tornado ranges between 17 and 19 m s^{-1}. The maximum intensity of the tornado can be estimated as IF2+ (67 m s^{-1} or 241 km h^{-1}).

2 http://www.keraunos.org/actualites/faits-marquants/2019/tornade-longwy-bascharage-9-aout-2019-meurthe-et-moselle-luxembourg-herserange-petange

3 https://www.facebook.com/permalink.php?story_fbid=2452220058133650&id=953889221300082

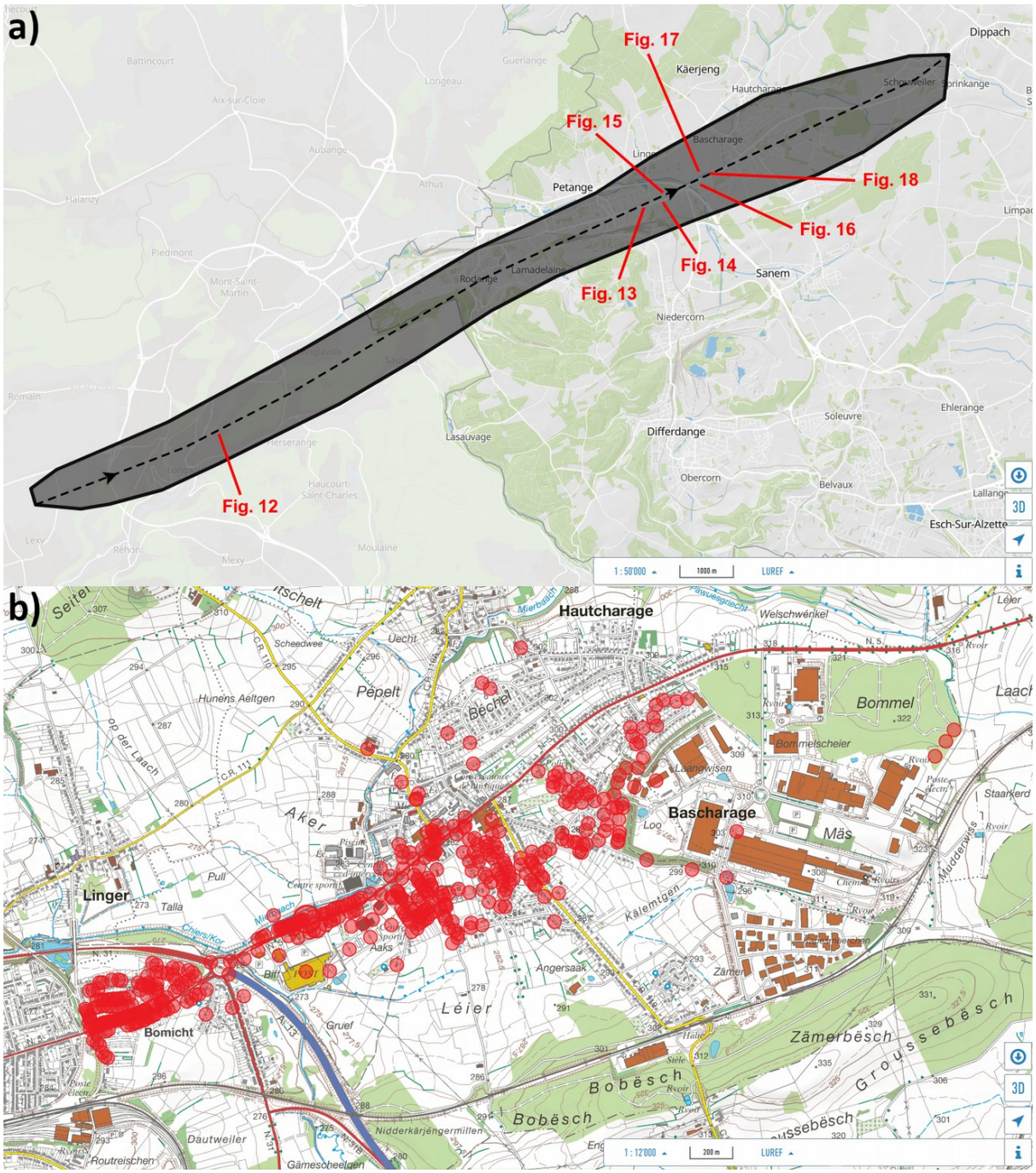

Figure 11: (a) Analysed track of the tornado with references of damage pictures shown in this study. Note that the width of the black polygon does not represent the true width of the tornado, but the estimated maximum damage radius. (b) Damage locations (red circles) in Bascharage mapped by the technical department of the municipality of Käerjeng. Source of base maps: National geoportal of Luxembourg.



Figure 12: The image shows a house with a clay tile roof in Herserange, where tiles have been blown off (Degree of Damage (DoD) 1). Assuming that the tiles were strongly attached, this would lead to a rating of IF1- to IF1 (36 to 41 m s^{-1} or 128 to 149 km h^{-1}). Photo: Réné Bych.



Figure 13: These are sturdy, standard terraced houses (sturdiness E) located in Pétange with significant damage to their roofs (DoD 1 to 2). This yields an estimate of IF2 to IF2+ or 54 to 67 m s^{-1} (217 - 241 km h^{-1}). Photo: Info Trafic Lorraine & Frontières.



Figure 14: Isolated and sturdy house (sturdiness E) located in Bascharage has lost its roof (DoD 2). This yields an estimate of IF2+ or 67 m s^{-1} (241 km h^{-1}). Photo: Claude Piscitelli.



Figure 15: A road vehicle/van (Damage Indicator (DI): V, sub-class: C) has been overturned and slightly displaced (DoD 2) in Bascharage, yielding an estimate of IF2- (54 m s^{-1} or 193 km h^{-1}). Photo: Info Trafic Lorraine & Frontières.



Figure 16: There are two damage indicators in this image showing a supermarket in Bascharage: a crushed pole with billboards on top and damage to two roofs. The billboard/pole can be rated using the DI S (signs and billboards). We have DoD 1 - collapse of pillar(s), which gives an estimated wind speed of 54 m s^{-1} (193 km h^{-1}) or IF2-. We have a building of sturdiness E (typical) with damage to a roof, but less than two thirds of the roof is damaged, which leads to an estimate of 60 m s^{-1} (217 km h^{-1}) or IF2. Photo: Luca Mathias.



Figure 17: A power transmission tower (DI: PT) has been deformed (DoD 1) in Bascharage, yielding an estimate of IF2 (60 m s^{-1} or 217 km h^{-1}). Photo: CGDIS.



Figure 18: These are sturdy, standard houses (sturdiness E) located in Bascharage with significant damage to their roofs (DoD 1 to 2). This yields an estimate of IF2 to IF2+ or 54 to 67 m s^{-1} (217 - 241 km h^{-1}). Photo: Dan Tempels.

7. SUMMARY AND CONCLUSIONS

The impactful tornado on 9 August 2019 in south-western Luxembourg was investigated with regard to the synoptic-scale and mesoscale meteorological context focusing on the atmospheric ingredients of this event. Furthermore, the evolution of the tornadic storm cell was thoroughly analysed and a rating of the tornadic wind damage is presented in this study.

The atmospheric setting was very conducive to the development of discrete and long-lived supercell thunderstorms over Luxembourg, north-eastern France, eastern Belgium and western Germany, where moderate latent instability and strong vertical wind shear overlapped ahead of a cold front. Moreover, due to the presence of a well-defined prefrontal mesoscale surface low, a significant amount of SRH was available in the lowest 3 km on the northern flank of this low pressure area. Together with high absolute and relative humidity in the boundary layer overlapping with 0-1 km SRH above 100 $m^2 s^{-2}$ in some areas, favourable lower-tropospheric conditions for mesocyclonic tornadogenesis were in place. In situ measurements from a weather station in the tornado environment indicated contamination of the relative humidity in the boundary layer by preceding precipitation, which may have have played a key role in conditioning the environment for tornadogenesis to some extent.

The radar analysis of the right-moving tornadic supercell revealed a long-lived mesocyclone, which strengthened while the storm was moving to Luxembourg. The intensification phase of the mesocyclonic updraft was characterised by a strong increase of the lightning activity The storm cell also exhibited a well-defined hook echo in the high-resolution radar imagery after the mesocyclone had strengthened. The formation of the hook echo signature preceded the tornadogenesis by about 10 minutes. Possible reasons for the tornadolysis were also proposed, which are the occlusion of the RFD and the collapse of the mesocyclonic updraft.

The estimation of the tornado intensity was based on damage pictures using the IF scale (Groenemeijer at al. 2018). The damage assessment yielded a rating of IF2+, which corresponds to a maximum wind speed of approximately 67 m s^{-1} (241 km h^{-1}). The tornado had an estimated path length of 18 to 20 km, whereas the damage path width reached its maximum in Bascharage. The rapid passage of the multi-vortex tornado through Rodange, Lamadelaine, Pétange and Bascharage was certainly one of the most damaging convective weather events in the Grand-Duchy of Luxembourg in decades. This hazardous event also highlights the necessity of doing further efforts regarding operational tornado forecasting and warnings in Europe, as pointed out by Rauhala and Schultz (2009) and Antonescu et al. (2017, 2018). Hence, MeteoLux has started an internal project to elaborate a concept for assessing the tornado risk associated with supercells during the warm season.



Figure 19: Picture of the damaging tornado taken from a location in Pétange while looking in a southerly direction. Source: https://www.wort.lu/de/lokales/100-haeuser-in-petingen-von-tornado-abgedeckt-5d4da009da2cc1784e3496d6

ACKNOWLEDGEMENTS

The author thanks Laurent Delobbe from RMIB for providing radar data and Bram van't Veen for assistance with the NLradar software. The author wants to thank ECMWF and Météo-France for the provision of NWP model data. The author thanks Stephan Thern from Siemens AG for providing EUCLID lightning data. The author also thanks the Kachelmann Group for archiving weather station data and making it freely available on its website (https://kachelmannwetter.com). The author thanks Guy Ferber from the technical department of the municipality of Käerjeng for sharing the mapped locations of damage in Bascharage. Finally, the author would like to thank Pieter Groenemeijer, Director of ESSL, for contributing to the damage assessment of the tornado.

REFERENCES

Antonescu, B., Schultz, D. M., Lomas, F., and Kühne, T. (2016): Tornadoes in Europe: Synthesis of the observational datasets. *Monthly Weather Review*, **144**, 2445-2480. DOI: https://doi.org/10.1175/MWR-D-15-0298.1

Antonescu, B., Schultz, D. M., Holzer, A., and Groenemeijer, P. (2017): Tornadoes in Europe: An Underestimated Threat. *Bulletin of the American Meteorological Society*, **98**, 713-728, DOI: https://doi.org/10.1175/BAMS-D-16-0171.1

Antonescu, B., Fairman, J. G., and Schultz, D. M. (2018): What is the Worst That Could Happen? Reexamining the 24–25 June 1967 Tornado Outbreak over Western Europe. *Weather, Climate and Society*, **10**, 323-340. DOI: https://doi.org/10.1175/WCAS-D-17-0076.1

Antonescu, B., Púčik, T., and Schultz, D. M. (2020): Hindcasting the First Tornado Forecast in Europe: 25 June 1967. *Weather and Forecasting*, **35**, 417-436. DOI: https://doi.org/10.1175/WAF-D-19-0173.1

Bunkers, M. J., Klimowski, B. A., Zeitler, J. W., Thompson, R. L., and Weisman, M. L. (2000): Predicting Supercell Motion Using a New Hodograph Technique. *Weather and Forecasting*, **15**, 61-79. DOI: https://doi.org/10.1175/1520-0434(2000)015<0061:PSMUAN>2.0.CO;2

Caniaux, G. (1984): Trombes et chutes de grêle du 20 septembre 1982 sur les Ardennes. Direction de la météorologie nationale, notes techniques n°8, Paris, 28 pp. [Available online: http://pluiesextremes.meteo.fr/france-metropole/IMG/sipex_pdf/1982_09_20_trombre_grele_ardennes.pdf]

Coffer, B. E., and Parker, M. D. (2017): Simulated Supercells in Nontornadic and Tornadic VORTEX2 Environments. *Monthly Weather Review*, **145**, 149-180, DOI: https://doi.org/10.1175/MWR-D-16-0226.1

Courtier, P., Freydier, C., Geleyn, J.-F., Rabier, F., and Rochas, M. (1991): The ARPEGE project at Météo-France, in: Workshop on numerical methods in atmospheric models. ECMWF, Reading, United Kingdom, 2, 193-232. [Available online: https://www.ecmwf.int/node/8798]

Dessens, J., and Snow, J. T. (1989): Tornadoes in France. *Weather and Forecasting*, **4**, 110-132. DOI: https://doi.org/10.1175/1520-0434(1989)004<0110:TIF>2.0.CO;2

Gemeng Käerjeng (2019): Eise Magazin - Spezialausgabe Tornado. [Available online: https://kaerjeng.lu/wp-content/uploads/2019/10/eise-magazin_SPECIAL_09-2019-BAT.pdf]

Groenemeijer, P., and Kühne, T. (2014): A climatology of tornadoes in Europe: Results from the European Severe Weather Database. *Monthly Weather Review*, **142**, 4775-4790. DOI: https://doi.org/10.1175/MWR-D-14-00107.1

Groenemeijer, P., and Coauthors (2018): The International Fujita (IF) Scale - Tornado and Wind Damage Assessment Guide. Draft Version 0.1, 48 pp. [Avalaible online: https://www.essl.org/cms/international-fujita-scale/]

Groenemeijer, P., Púčik, T., Tsonevsky, I., and Bechtold, P. (2019): An Overview of Convective Available Potential Energy and Convective Inhibition provided by NWP models for operational forecasting. ECMWF, Technical Memorandum No.852, 19 pp. DOI: http://dx.doi.org/10.21957/q392hofrl

Hengstebeck, T., Wapler, K., Heizenreder, D., and Joe, P. (2018): Radar Network–Based Detection of Mesocyclones at the German Weather Service. *Journal of Atmospheric and Oceanic Technology*, **35**, 299-321. DOI: https://doi.org/10.1175/JTECH-D-16-0230.1

Johns, R. H., and Doswell III, C. A. (1992): Severe local storms forecasting. *Weather and Forecasting*, **7**, 588-612. DOI: https://doi.org/10.1175/1520-0434(1992)007%3C0588:SLSF%3E2.0.CO;2

Kain, J. S., and Coauthors (2008): Some Practical Considerations Regarding Horizontal Resolution in the First Generation of Operational Convection-Allowing NWP. *Weather and Forecasting*, **23**, 931-952. DOI: https://doi.org/10.1175/WAF2007106.1

Markowski, P. M., Straka, J. M., Rasmussen, E. N., and Blanchard, D. O. (1998): Variability of Storm-Relative Helicity during VORTEX. *Monthly Weather Review*, **126**, 2959-2971, DOI: https://doi.org/10.1175/1520-0493(1998)126<2959:VOSRHD>2.0.CO;2

Markowski, P. M., and Richardson, Y. P. (2009): Tornadogenesis: Our current understanding, forecasting considerations, and questions to guide future research. *Atmospheric Research*, **93**, 3-10. DOI: https://doi.org/10.1016/j.atmosres.2008.09.015

Markowski, P. M., and Richardson, Y. P. (2014a): What we know and what we don't know about tornado formation. *Physics Today*, **67**(9), 26-31. DOI: https://doi.org/10.1063/PT.3.2514

Markowski, P. M., and Richardson, Y. P. (2014b): The Influence of Environmental Low-Level Shear and Cold Pools on Tornadogenesis: Insights from Idealized Simulations. *Journal of Atmospheric Sciences*, **71**, 243-275, DOI: https://doi.org/10.1175/JAS-D-13-0159.1

Pédeboy, S., Defer, E., and Schulz, W. (2014): Performance of the EUCLID network in cloud lightning detection in the South-East France. 8th HyMeX Workshop, Valletta, Malta. [Available online: https://www.hymex.org/?page=public/workshops/8/programme#Posters]

Púčik, T., Groenemeijer, P., Rýva, D., and Kolář, M. (2015): Proximity soundings of severe and nonsevere thunderstorms in central Europe. *Monthly Weather Review*, **143**, 4805-4821. DOI: https://doi.org/10.1175/MWR-D-15-0104.1

Rasmussen, E. N., and Blanchard, D. O. (1998): A baseline climatology of sounding-derived supercell and tornado forecast parameters. *Weather and Forecasting*, **13**, 1148-1164. DOI: https://doi.org/10.1175/1520-0434(1998)013%3C1148:ABCOSD%3E2.0.CO;2

Schulz, W., Pédeboy, S., Vergeiner, C., Defer, E., and Rison, W. (2014): Validation of the EUCLID LLS during HyMeX SOP1. International Lightning Detection Conference and International Lightning Meteorology Conference (ILDC/ILMC), Tucson, Arizona, USA, 2-5. [Available online: https://tinyurl.com/y8gs96k9]

Schulz, W., Diendorfer, G., Pédeboy, S., and Poelman, D. R. (2016): The European lightning location system EUCLID – Part 1: Performance analysis and validation. *Natural Hazards and Earth System Sciences*, **16**, 595-605. DOI: https://doi.org/10.5194/nhess-16-595-2016

Seity, Y., Brousseau, P., Malardel, S., Hello, G., Bénard, P., Bouttier, F., Lac, C., and Masson, V. (2011): The AROME-France Convective-Scale Operational Model. *Monthly Weather Review*, **139**, 976-991. DOI: https://doi.org/10.1175/2010MWR3425.1

Taszarek, M., Brooks, H. E., and B. Czernecki, B. (2017): Sounding-Derived Parameters Associated with Convective Hazards in Europe. *Monthly Weather Review*, **145**, 1511-1528. DOI: https://doi.org/10.1175/MWR-D-16-0384.1

Thompson, R. L., Edwards, R., Hart, J. A., Elmore, K. L., and Markowski, P. (2003): Close proximity soundings within supercell environments obtained from the Rapid Update Cycle. *Weather and Forecasting*, **18**, 1243-1261. DOI: https://doi.org/10.1175/1520-0434(2003)018%3C1243:CPSWSE%3E2.0.CO;2

Thompson, R. L., Edwards, R., and Mead, C. M. (2004): An update to the supercell composite and significant tornado parameters. Preprints, 22nd Conf. Severe Local Storms, Hyannis, MA, American Meteorological Society, P8.1. [Available online : https://ams.confex.com/ams/11aram22sls/techprogram/paper_82100.htm]

Tuschy, H. (2009): Examination of severe thunderstorm outbreaks in Central Europe. Master thesis, Institute of Meteorology and Geophysics, University of Innsbruck, Austria, 204 pp. [Available online: https://www.uibk.ac.at/acinn/theses/diploma-theses/tuschy_helge_2009_dipl.pdf]

Trierischer Volksfreund (2008): 20 Jahre danach - Wirbelsturm über Trier. [Available online: https://tornadoliste.de/bilder/1988/081007tv.pdf]

Wapler, K., Hengstebeck, T., and Groenemeijer, P. (2016): Mesocyclones in Central Europe as seen by radar. *Atmospheric Research,* **168**, 112-120. DOI: https://doi.org/10.1016/j.atmosres.2015.08.023

Wesolek, E., and Mahieu, P. (2011): The F4 tornado of August 3, 2008, in Northern France: Case study of a tornadic storm in a low CAPE environment. *Atmospheric Research*, **100**, 649-656. DOI: https://doi.org/10.1016/j.atmosres.2010.09.003

Yokota, S., Niino, H., Seko, H., Kunii, M., and Yamauchi, H. (2018): Important Factors for Tornadogenesis as Revealed by High-Resolution Ensemble Forecasts of the Tsukuba Supercell Tornado of 6 May 2012 in Japan. *Monthly Weather Review*, **146**, 1109-1132. DOI: https://doi.org/10.1175/MWR-D-17-0254.1